

## Dynamics and decoherence in the central spin model using exact methods

Michael Bortz,<sup>1,2,\*</sup> Sebastian Eggert,<sup>1</sup> Christian Schneider,<sup>3</sup> Robert Stübner,<sup>4</sup> and Joachim Stolze<sup>4</sup>

<sup>1</sup>Physics Department and Research Center OPTIMAS, Technische Universität Kaiserslautern, 67663 Kaiserslautern, Germany

<sup>2</sup>Fraunhofer ITWM, 67663 Kaiserslautern, Germany

<sup>3</sup>IfB, HIF E12, ETH Hönggerberg, 8093 Zürich, Switzerland

<sup>4</sup>Technische Universität Dortmund, Fakultät Physik, 44221 Dortmund, Germany

(Received 23 September 2010; published 19 October 2010)

The dynamics and decoherence of an electronic spin-1/2 qubit coupled to a bath of nuclear spins via hyperfine interactions in a quantum dot is studied. We show how exact results from the integrable solution can be used to understand the dynamic behavior of the qubit. It is possible to predict the main frequency contributions and their broadening for relatively general initial states analytically, leading to an estimate of the corresponding decay times, which are related to  $T_1$  of the electron. Furthermore, for a small bath polarization, a distinct low-frequency time scale is observed.

DOI: [10.1103/PhysRevB.82.161308](https://doi.org/10.1103/PhysRevB.82.161308)

PACS number(s): 73.21.La, 76.60.-k, 02.30.Ik, 03.65.Yz

One of the most challenging tasks in both theoretical and experimental studies of quantum-information processing is the understanding and control of decoherence due to the interaction with the environment. A prototypical example for the loss of quantum information is an electron trapped in a quantum dot, surrounded by nuclear spins. On short-time scales up to 1 ms,<sup>1</sup> the Heisenberg exchange resulting from the hyperfine interaction between the electron and the nuclei dominates, before spin-orbit coupling or dipole-dipole interactions between the bath spins become effective.<sup>2,3</sup> Indeed, impressive experimental progress has been made over the recent years to observe and control oscillations of single electron spins coupled to bath spins by various techniques.<sup>4–8</sup> In a typical magnetic-resonance experiment, for example, one applies a static magnetic field creating a Zeeman splitting of the spin's energy levels, plus a resonant or near resonant alternating field transverse to the Zeeman field. Spin-rotation angles can then be controlled, e.g., by the duration of the transverse field pulse. The decoherence processes on which we focus here, however, are not directly linked to the applied fields but are instead caused mainly by the Heisenberg coupling to the nuclear bath spins, which is given by Hamiltonian

$$H = \sum_{j=1}^{N_b} A_j \mathbf{S}_0 \cdot \mathbf{S}_j, \quad (1)$$

where  $N_b$  is the number of bath spins and  $\mathbf{S}_0$  is the central electron spin. This so-called central spin model is one of the most studied theoretical models for decoherence,<sup>9–18</sup> which can also be treated by exact methods.<sup>19–21</sup> In this Rapid Communication, we are interested in an analytic understanding of the detailed decoherence-induced dynamics of  $\langle S_0^z \rangle(t)$  due to the coupling to the spin bath. We therefore do not consider any external magnetic fields but instead specify the initial overall polarization of the system, which is conserved. The central spin  $\mathbf{S}_0$  is initially assumed to be in its down state, independent of the bath spins. This initial product state gets entangled by the exchange interactions, leading to the decoherence of the central spin.

The couplings  $A_j > 0$  in Eq. (1) are proportional to the square of the electronic wave function at the position of the nucleus  $j$ . The methods we apply in the following do not depend on the special choice of the  $A_j$ . For definiteness, we assume a Gaussian distribution with the site index (distance)  $j$  (Refs. 13 and 21)

$$A_j = \frac{x_1 N_b \exp[-(jB/N_b)^2]}{\sum_{j=1}^{N_b} \exp[-(jB/N_b)^2]}, \quad (2)$$

which allows an easy control over the two relevant characteristics of the distribution of  $A_j$ , namely, the mean value  $x_1 = \frac{1}{N_b} \sum_j A_j$  and the degree of inhomogeneity as parametrized by  $B$ . Generally the results are largely insensitive to the overall shape of the distribution, (e.g., in case a higher-dimensional site index is used) as long as the mean  $x_1$  and the degree of inhomogeneity are the same.

For homogeneous couplings,  $A_j \equiv A \forall j$ , a nontrivial time scale  $\tau \sim A^{-1} N_b^{-1/2}$  has been identified using exact methods,<sup>22,23</sup> which can be interpreted as a decoherence time. A number of authors<sup>3,10–18</sup> have studied the influence of inhomogeneous couplings by a variety of approximate numerical and analytical methods. Obviously the use of exact Bethe Ansatz methods to the general dynamic problem would be a great advantage but so far the possibilities have been limited to certain nonequilibrium situations in the related BCS model<sup>24</sup> and to the special case of a maximal bath polarization.<sup>20</sup> Here we demonstrate how Bethe Ansatz results can be used to obtain the central features of the dynamic behavior for more general polarizations and coupling constants and compare with numerical complete diagonalization results.

We first want to consider an initial state  $|L\rangle = |\downarrow, \uparrow, \uparrow, \downarrow, \dots, \uparrow\rangle$ , where the central spin  $\downarrow$  and  $M_b$  bath spins at specified sites  $L = \{\ell_1, \dots, \ell_{M_b}\}$  are in the down state. All other spins are in the up state. Hence  $|L\rangle$  is an eigenstate of all  $S_i^z$  operators with total magnetization  $S_{\text{tot}}^z = N_b/2 - M_b - 1/2$  and is initially not entangled in any way. The time evolution is given in terms of the eigenstates  $|M_\nu\rangle$  and eigenvalues  $\Lambda_{M_\nu}$  of the model (1)

$$|L(t)\rangle = \sum_{\nu} e^{-i\Lambda_{M_{\nu}} t} |M_{\nu}\rangle \langle M_{\nu}|L\rangle. \quad (3)$$

From Eq. (3) an explicit expression for the reduced density matrix of the central spin can be derived,<sup>20</sup> which we employ to evaluate

$$\langle S_0^z \rangle(t) = \frac{1}{2} \left( 1 - 2 \sum_J |c_J(t)|^2 \right) \quad (4)$$

with

$$\alpha_J(t) = \langle J|L(t)\rangle = \sum_{\nu} \langle J|M_{\nu}\rangle \langle M_{\nu}|L\rangle e^{-i\Lambda_{M_{\nu}} t}, \quad (5)$$

where both  $|L\rangle$  and  $|J\rangle$  are eigenstates of all  $S_i^z$  with the central spin fixed in the down state. Thus it suffices to specify only the  $M_b$  flipped bath spins in the subsector of dimension  $C_{M_b}^{N_b} = N_b! / [(N_b - M_b)! M_b!]$ . In Ref. 20 the matrix elements  $\langle M_{\nu}|L\rangle$  were explicitly given in terms of the quantum numbers (Bethe roots, see below) of the energy eigenstates  $|M_{\nu}\rangle$  and of the  $S_i^z$  eigenstates  $|L\rangle$ ; alternatively, they can be obtained from a complete diagonalization. However, an exact calculation of the large number of terms in the sums, Eqs. (4) and (5), is impossible already for modest system sizes, except for special cases. In particular, a fully polarized bath  $S_{\text{tot}}^z = N_b/2 - 1/2$  (i.e.,  $M_b = 0$ ) was studied in Refs. 10 and 20, where the sum in Eq. (5) only contains  $N_b + 1$  terms.

We now would like to consider a more general polarization,  $M_b \neq 0$ , and single out the most important contributions to the sum, Eq. (5). In this way, it is possible to estimate the dominant frequency scales and the widths of peaks in the frequency spectrum of Eq. (4) and thus to obtain the decoherence time. Our strategy is based on results in Ref. 21, where it was found that only a few product states  $|J\rangle$  have an appreciable overlap  $\langle J|M_{\nu}\rangle$  for a given  $|M_{\nu}\rangle$  as long as  $M_b \ll N$ . These product states are essentially those obtained from the classical ground state  $|\downarrow, \uparrow, \uparrow, \dots, \uparrow\rangle$  by flipping certain individual nuclear bath spins as outlined below, that spin pattern being also reflected in the local expectation values  $\langle S_j^z \rangle$ .<sup>21</sup> We illustrate this method for  $M_b = 1$  first and generalize the results afterward.

The eigenstates  $|M_{\nu}\rangle$  can be classified by a set of  $M_b + 1$  Bethe roots  $\{\omega_{0,\nu}, \dots, \omega_{M_b,\nu}\}$  of the exact solution. Their positions in the complex plane are determined by coupled nonlinear equations.<sup>19,20</sup> The eigenvalues are given by

$$\Lambda_{M_{\nu}} = -\frac{1}{2} \sum_{k=0}^{M_b} \omega_{k,\nu} + \frac{N_b x_1}{4}. \quad (6)$$

To each eigenstate belongs a distinct root pattern that is related to the flipped spins relative to the all up state.<sup>21</sup> In particular, a Bethe root in the origin corresponds approximately to the application of a global lowering operator  $S_{\text{tot}}^-$ , a root  $A_{\ell+1} < \omega < A_{\ell}$  induces essentially a superposition of states with spin flips on sites  $\ell, \ell+1$  (Ref. 25) and a root  $\omega = \mathcal{O}(N_b)$  mainly causes a flip of the central spin, respectively. Therefore, for  $M_b = 1$  the state with the central spin and a single bath spin at site  $\ell$  in the down state is most

strongly overlapping with the six eigenstates that are characterized by two Bethe roots as follows:  $|0, 0\rangle$ ,  $|0, \omega_{1,\ell-1}\rangle$ ,  $|0, \omega_{1,\ell}\rangle$ ,  $|0, \tilde{\omega}_0\rangle$ ,  $|\omega'_{1,\ell}, \omega_{0,\ell}\rangle$ , and  $|\omega'_{1,\ell-1}, \omega_{0,\ell-1}\rangle$ , where the roots can be approximately determined from the distribution of  $A_j$  in an expansion of  $d := (N_b x_1)^{-1}$  and  $y_1 := d \sum_{j=1}^{N_b} A_j^2$  as<sup>21</sup>

$$\begin{aligned} \tilde{\omega}_0 &= 1/d + y_1 + \mathcal{O}(d), \\ \omega_{0,\ell} &= 1/d + y_1 - 2A_{\ell} + \mathcal{O}(d), \\ \omega_{1,\ell} &\approx \omega'_{1,\ell} = A_{\ell} + \mathcal{O}(d). \end{aligned} \quad (7)$$

The sum of the squared overlaps  $|\langle M_{\nu}|L\rangle|^2$  from only those states yields 0.71 for  $\ell = 1$  increasing to 0.96 for  $\ell = N_b$  (Ref. 25) in a system with  $N_b = 15$  and  $x_1 = B = 2$  in Eq. (2). Therefore, most of the weight in the expansion of  $|L\rangle$  into eigenstates is indeed found by only considering the six states listed above. For more homogeneous couplings ( $B = 0.4$ ) the corresponding overlaps are significantly larger.

Once these most important contributing states are known, the actual values of the overlaps  $\langle M_{\nu}|L\rangle$  are secondary but the differences in the corresponding eigenvalues  $\Lambda_{M_{\nu}}$  determine the spectral distribution in Eqs. (4) and (5) and therefore the decay time. Taking the corresponding differences of eigenvalues using Eqs. (4)–(7), we find that the high-frequency contributions occur at  $\Omega_0 = \frac{1}{2d}(1 + dy_1)$  and in an interval  $[\Omega_{1,\ell} - \Delta_{\ell}/2, \Omega_{1,\ell} + \Delta_{\ell}/2]$  around the  $\ell$ -dependent frequency  $\Omega_{1,\ell} = \frac{1}{2d}(1 + dy_1 - 2dA_{\ell})$ , where  $\Delta_{\ell} := (A_{\ell-1} - A_{\ell+1})/2$  up to terms of order  $\mathcal{O}(d)$ . The long time-scale  $\sim 1/\Delta_{\ell}$  resulting from the width of the peak near  $\Omega_{1,\ell}$  can accordingly be interpreted as the decoherence time for this dominant oscillation. In addition, there are low-frequency contributions around  $\Omega_{2,\ell} = A_{\ell}/2 + \mathcal{O}(d)$  due to the inhomogeneity in the couplings  $A_j$ , which disappear for a homogeneous model.<sup>22</sup>

Before turning to other polarizations,  $M_b > 1$ , we can now also consider more realistic initial states with bath configurations other than the  $S_i^z$  product eigenstates hitherto considered. In the following we will use a uniform distribution over all bath states with a given polarization as the initial state, given by the density matrix

$$\rho_t = (C_{M_b}^{N_b})^{-1} |\downarrow\rangle\langle\downarrow| \mathbb{1}_{M_b}, \quad (8)$$

where  $\mathbb{1}_{M_b}$  is the projection operator onto the sector with  $M_b$  flipped bath spins relative to the fully polarized up state. In this case the frequency spectrum of  $\langle S_0^z \rangle(t)$  consists of the superposition of the spectra obtained for all allowed individual product states. Thus for  $M_b = 1$ , all frequencies  $\Omega_{1,\ell}, \Omega_{2,\ell}$  contribute with  $\ell = 1, \dots, N_b$ . Thus the high-frequency spectrum now consists of one sharp peak at  $\Omega_0$  and of a second peak at  $\Omega_1 := \Omega_0 - x_1$  with a width  $\Delta := A_1 - A_{N_b}$ . Accordingly, the corresponding decoherence time for this oscillation is given by

$$\tau = 2\pi/\Delta, \quad (9)$$

which is therefore directly linked to the inhomogeneity of couplings. Another way of interpreting these results is to say that the central spin precesses in the effective field from the coupled bath state with a relaxation time  $T_1 \sim \tau$ . The low-

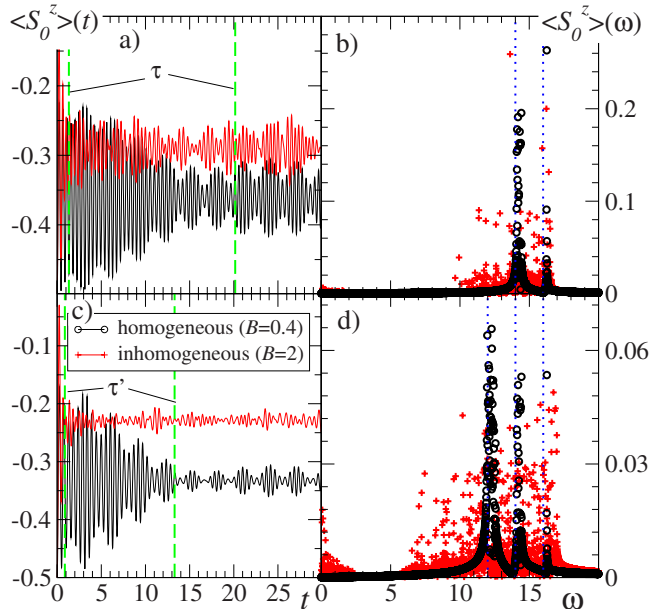


FIG. 1. (Color online) Time evolution  $\langle S_0^z \rangle(t)$  [(a) and (c)] and the corresponding Fourier transform [ $\langle S_0^z \rangle(\omega)$ ] for  $N_b=15$ ,  $x_1=2$ , and an initial uniform distribution of bath states with  $M_b=1$  [in (a) and (b)] and  $M_b=2$  [in (c) and (d)], respectively. The effect of two different homogeneity parameters  $B=0.4$  (circles, black, lower time series) and  $B=2$  (crosses, red, upper time series) for the couplings in Eq. (2) is shown. Dashed lines (green) show the estimates for the decoherence times. The dotted lines (blue) give the position of the peaks in the homogeneous limit  $A_j=2$ .

frequency tail contains frequencies in the interval  $[A_{N_b}, A_1]$ .

In order to illustrate the decoherence process, we show the time evolution of  $\langle S_0^z \rangle(t)$  and the corresponding Fourier transform  $\langle S_0^z \rangle(\omega)$  for  $N_b=15$  bath spins as obtained from complete diagonalization in Fig. 1. We choose  $x_1=2$  and two different values for  $B$ , corresponding to relatively homogeneous ( $B=0.4$ ) and relatively inhomogeneous ( $B=2$ ) couplings in Eq. (2). For nearly homogeneous couplings, the broadening of the peak near  $\Omega_1$  is demonstrated nicely. For  $B=2$ , the two peaks cannot be distinguished any longer due to the large broadening of the peak around  $\Omega_1$ .

We can generalize the above discussion to larger  $M_b$  with the analogous initial density matrix in Eq. (8). For  $M_b=2$  three peaks are present centered around  $\Omega_0$  and  $\Omega_1$  as given above and around  $\Omega_2 := \Omega_0 - 2x_1$ . Neglecting complex string solutions of the Bethe Ansatz equations and interactions between excitations, one expects the peak near  $\Omega_2$  to have twice the width  $\Delta_2=2\Delta$ . Again, in the homogeneous limit, the known<sup>20</sup> frequencies  $A(N_b+1-2k)$ ,  $k=0,1,2$ , are recovered. From the beating of oscillations within the corresponding frequency ranges we estimate the overall decoherence time to be  $\tau'=2\tau/3$ . The results for  $M_b=2$  in Fig. 1 are consistent with the estimates for  $\tau$  and  $\tau'$ . At the same time, one notices that additional spectral weight develops at small frequencies for increasing  $M_b$  for inhomogeneous couplings. This can be traced back to the combination of states with Bethe roots  $(0, \omega'_{1,\ell})$  and  $(0,0)$  in the sum in Eq. (4). Therefore, the smallest of these resulting frequencies is given by the most weakly coupled spins,  $\Omega \sim A_{N_b}/2$ , around which

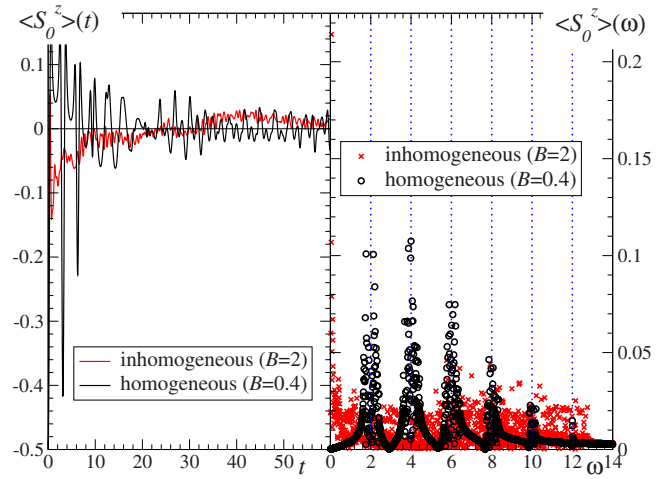


FIG. 2. (Color online) The time evolution  $\langle S_0^z \rangle(t)$  (left) and its Fourier transform  $\langle S_0^z \rangle(\omega)$  for  $S_{\text{tot}}^z=0$  from complete diagonalization, for  $N_b=11$ ,  $x_1=2$ , and two different choices of the homogeneity parameter  $B$  in Eq. (2). The dotted lines (blue) give the position of the peaks in the homogeneous limit  $A=2$ . The smaller amplitude oscillations in the left panel correspond to the inhomogeneous case  $B=2$ .

indeed most of the spectral weight in the low-frequency region of Fig. 1(d) develops.

It is possible to increase  $M_b$  further and continue this analysis with more peaks for other initial bath configurations as long as  $M_b \ll N_b$ . The positions and widths of the peaks directly reflect the initially flipped bath spins and the choice of couplings. For larger  $M_b$ , however, interactions between the elementary excitations may distort the simple analogy between roots and flipped spins above. Therefore, we analyze the situation in the following for small bath magnetization  $M_b \sim N_b/2$  using complete diagonalization on a smaller system in order to see which features of the analytic considerations can survive in that case.

In Fig. 2, we show results for  $N_b=11$  in the subsector  $S_{\text{tot}}^z=0$ , where we took the average over all allowed product states as in Eq. (8) with the central spin pointing down. For a weak inhomogeneity, one can still clearly distinguish the discrete peaks in the Fourier transform, so that the analytical predictions are still useful for  $M_b=5$  in this case. The decoherence times of the lower frequency oscillations are again generally shorter, as can be seen by the widths of the corresponding peaks.

This structure is lost for couplings with a significant degree of inhomogeneity, i.e., when the difference in couplings becomes larger than the peak separation. However, as can be seen both in the time evolution and its Fourier transform, a new time scale at small energies occurs, which leads to low-frequency oscillations. In the Fourier transform, this shows up as a relatively strong peak at low frequency. It is reasonable to expect that this stems from the same low-frequency mechanism as discussed above, namely, the overlap between the ground state—with all roots in the origin except for  $\omega_0$ —and the lowest excited state—where one root is shifted out of the origin into the interval between  $A_{N_b}$  and  $A_{N_b-1}$ . This yields dominant frequencies corresponding to the most

weakly coupled spins,  $\Omega \sim A_{N_b}/2$ , leading to a characteristic long-time oscillation  $4\pi/A_{N_b}$ . The physical interpretation is that for generic disordered couplings fluctuations occur on all time scales up to the highest frequencies  $\Omega_0 \sim \sum_j A_j$  leading to a correspondingly large  $1/T_1$  but for longer times there remains a relatively coherent low-frequency oscillation, which emphasizes the importance of the weakly coupled nuclear bath spins in the time evolution of the central spin.<sup>18</sup> This long-time behavior can be explained by realizing that the most weakly coupled spins simply play the role of a relatively stable background field but never actually become strongly entangled with the rest of the system.

In summary, we have analyzed the decoherence in the commonly used central spin model using exact methods. For relatively homogeneous couplings the locations and widths of dominant oscillations in the Fourier spectrum  $\langle S_0^z \rangle(\omega)$  can be predicted analytically even for smaller polarizations (large  $M_b$ ). The positions and widths of the peaks directly reflect the initial bath state and the choice of couplings. High-frequency oscillations have the longest decoherence times. For larger inhomogeneity in the couplings the decoherence times become shorter and eventually the simple peak structure is lost. However, in this case the appearance of a low-

frequency feature can again be inferred from the root structure of the exact solution. Accordingly, it is possible to identify the physical behavior of the dynamics in the different cases, namely fast oscillations with decoherence due to the difference in coupling strengths for nearly homogeneous couplings on the one hand and relatively stable long-time oscillations due to the most weakly coupled background for inhomogeneous couplings on the other hand. The results also provide a direct link from clear signatures in the dynamics to individual excitations and characteristics of the model. This opens different possibilities and insights for the analysis of the dynamical behavior that can be obtained from independent methods, e.g., from more advanced numerical or even experimental studies.

We are grateful to F. H. L. Essler, F. Göhmann, A. Klümper, I. Schneider, and A. Struck for useful discussions. M.B. thanks the Rudolf-Peierls-Centre for Theoretical Physics, University of Oxford, for kind hospitality. Financial support by the European network INSTANS and the DFG via the research initiative SFB-TR49 is gratefully acknowledged.

\*michael.bortz@itwm.fraunhofer.de

- <sup>1</sup>A. C. Johnson, J. R. Petta, J. M. Taylor, A. Yacoby, M. D. Lukin, C. M. Markus, M. P. Hanson, and A. C. Gossard, *Nature (London)* **435**, 925 (2005).
- <sup>2</sup>A. V. Khaetskii and Y. V. Nazarov, *Phys. Rev. B* **61**, 12639 (2000); **64**, 125316 (2001).
- <sup>3</sup>J. Schliemann, A. V. Khaetskii, and D. Loss, *J. Phys.: Condens. Matter* **15**, R1809 (2003).
- <sup>4</sup>F. Jelezko, T. Gaebel, I. Popa, A. Gruber, and J. Wrachtrup, *Phys. Rev. Lett.* **92**, 076401 (2004).
- <sup>5</sup>J. Berezovsky, M. H. Mikkelsen, N. B. Stoltz, L. A. Coldren, and D. D. Aschwalom, *Science* **320**, 349 (2008).
- <sup>6</sup>D. Press, T. D. Ladd, B. Thang, and Y. Yamamoto, *Nature (London)* **456**, 218 (2008).
- <sup>7</sup>R. Hanson, V. V. Dobrovitski, A. E. Feiguin, O. Gywat, and D. D. Aschwalom, *Science* **320**, 352 (2008).
- <sup>8</sup>A. Greilich, S. E. Economou, S. Spatzek, D. R. Yakovlev, D. Reuter, A. D. Wieck, T. L. Reinecke, and M. Bayer, *Nat. Phys.* **5**, 262 (2009).
- <sup>9</sup>N. V. Prokof'ev and P. C. E. Stamp, *Rep. Prog. Phys.* **63**, 669 (2000).
- <sup>10</sup>A. V. Khaetskii, D. Loss, and L. Glazman, *Phys. Rev. Lett.* **88**, 186802 (2002); *Phys. Rev. B* **67**, 195329 (2003).
- <sup>11</sup>J. Schliemann, A. V. Khaetskii, and D. Loss, *Phys. Rev. B* **66**, 245303 (2002).
- <sup>12</sup>V. V. Dobrovitski and H. A. De Raedt, *Phys. Rev. E* **67**, 056702 (2003).
- <sup>13</sup>W. A. Coish and D. Loss, *Phys. Rev. B* **70**, 195340 (2004).
- <sup>14</sup>S. I. Erlingsson and Y. V. Nazarov, *Phys. Rev. B* **70**, 205327 (2004).
- <sup>15</sup>K. A. Al-Hassanieh, V. V. Dobrovitski, E. Dagotto, and B. N. Harmon, *Phys. Rev. Lett.* **97**, 037204 (2006).
- <sup>16</sup>W. A. Coish, E. A. Yuzbashyan, B. L. Altshuler, and D. Loss, *J. Appl. Phys.* **101**, 081715 (2007).
- <sup>17</sup>C. Deng and X. Hu, *Phys. Rev. B* **73**, 241303(R) (2006).
- <sup>18</sup>G. Chen, D. L. Bergman, and L. Balents, *Phys. Rev. B* **76**, 045312 (2007).
- <sup>19</sup>M. Gaudin, *La fonction d'onde de Bethe* (Masson, Paris, 1983).
- <sup>20</sup>M. Bortz and J. Stolze, *Phys. Rev. B* **76**, 014304 (2007).
- <sup>21</sup>M. Bortz, S. Eggert, and J. Stolze, *Phys. Rev. B* **81**, 035315 (2010).
- <sup>22</sup>M. Bortz and J. Stolze, *J. Stat. Mech.: Theory Exp.* (2007) P06018.
- <sup>23</sup>G. G. Kozlov, *Sov. Phys. JETP* **105**, 803 (2007).
- <sup>24</sup>A. Faribault, P. Calabrese, and J.-S. Caux, *J. Stat. Mech.: Theory Exp.* (2009) P03018.
- <sup>25</sup>The correspondence of roots to local spin flips is particularly good for the more loosely bound spins  $\ell \gg 1$ .